International Journal of Advanced Engineering, Management and Science (IJAEMS)
Peer-Reviewed Journal
ISSN: 2454-1311 | Vol-12, Issue-3; May-Jun, 2026
Journal Home Page: https://ijaems.com/
DOI: https://dx.doi.org/10.22161/ijaems.123.6

Investigating Spatiotemporal Land Cover Changes in the Bahr El Jebel Basin Using Remote Sensing

Ahmed Y. Abed[1], Aly N. El-Bahrawy[2], Eman Soliman[3], Amr Fawzy[4] and Hoda Soussa[5]

[1]Nile Water Sector, Ministry of Water Resources and Irrigation, Cairo, Egypt
Email: eng_yassin_2022@yahoo.com
[2]Irrigation and Hydraulics Department, Faculty of Engineering, Ain Shams University, Cairo, Egypt
alyelbahrawy@yahoo.com
[3]Water Management, Food and Agriculture Organization of the United Nations, Riyadh, Saudi Arabia
eman_sayed@hotmail.com
[4]Strategic Planning Sector, Ministry of Water Resources and Irrigation, Cairo, Egypt
amrfma@hotmail.com
[5]Irrigation and Hydraulics Department, Faculty of Engineering, Ain Shams University, Cairo, Egypt
Hoda_soussa@eng.asu.edu.eg

Received: 05 Apr 2026; Received in revised form: 30 Apr 2026; Accepted: 03 May 2026; Available online: 09 May 2026

Abstract *— This research examines spatiotemporal land cover changes in the Bahr El Jebel Basin using remote sensing, with emphasis on wetland-related classes and their hydro-climatic controls. Land use/land cover dynamics were derived from Dynamic World data based on Sentinel-2 imagery. Rainfall variability was assessed using CHIRPS, actual evapotranspiration was obtained from WaPOR, and water levels in Lakes Victoria, Kyoga, and Albert were used as indicators of upstream hydrological forcing from the Equatorial Lakes system.*

The results show clear land cover changes across the basin, particularly in swamp and flooded vegetation classes. The year 2019 marked a major transition, after which wetland-related land cover expanded noticeably. Rainfall anomaly analysis indicated wetter-than-normal conditions in both the Bahr El Jebel reach and the Equatorial Lakes sub-basin during 2019 and the following years. At the same time, lake levels in the Equatorial Lakes system increased, indicating stronger upstream storage and downstream flow support. In contrast, the precipitation–evapotranspiration analysis showed that evapotranspiration exceeded precipitation during most months, suggesting that local rainfall alone was insufficient to maintain flooded vegetation.

The findings indicate that the recent expansion of flooded vegetation in the Bahr El Jebel Basin was driven mainly by upstream inflows from the Equatorial Lakes system, while local rainfall played a secondary role. The study demonstrates the usefulness of remote sensing for monitoring land cover dynamics in data-scarce wetland basins.

Keywords *— **Bahr El Jebel Basin, Equatorial Lakes, flooded vegetation, land cover change, remote sensing.***

I. INTRODUCTION

The Bahr El Jebel Basin forms a critical part of the Upper Nile system and represents the upper segment of the White Nile, extending from the Uganda–South Sudan border northward through the Sudd wetland, one of the world's largest tropical freshwater wetland complexes (Nile Basin Initiative, 2020). The basin is characterized by exceptionally flat topography, extensive seasonal flooding, and strong hydrological interactions among river inflow,

rainfall, evapotranspiration, and wetland vegetation (Petersen & Fohrer, 2010). Owing to its ecological and hydrological significance as both a regulator of Nile flows and a reservoir of biodiversity, understanding Land Use and Land Cover (LULC) dynamics within this reach has attracted sustained scientific attention. In particular, the spatial and temporal expansion and contraction of flooded vegetation remain insufficiently constrained in terms of their principal drivers, with previous studies variously attributing observed changes to local land management, climate variability, or upstream hydrological forcing. These conditions make the basin highly dynamic in both space and time, with land cover patterns that are highly sensitive to hydrological variability and environmental change (Denny, 1984; NBI, 2020).

Understanding land cover dynamics in the Bahr El Jebel Basin is important not only from an ecological perspective, but also for water resources assessment, wetland monitoring, and basin-scale environmental planning. In floodplain systems such as the Sudd, land cover is closely linked to the seasonal expansion and contraction of inundated areas (Rebelo et al., 2012). It is also associated with the spatial distribution of open water, flooded vegetation, grasslands, shrublands, and other wetland-related classes (Di Vittorio & Georgakakos, 2018). Therefore, changes in land cover can provide valuable insight into broader hydro-climatic shifts and environmental responses across the basin (Persico et al., 2024).

Previous studies in the Sudd area have demonstrated the strong value of remote sensing for investigating wetland and floodplain dynamics in this otherwise inaccessible environment. Early work by Denny (1984) documented the ecological structure of permanent swamp vegetation in the Upper Nile and provided a baseline understanding of wetland plant communities. Later, Petersen et al. (2007) used remote sensing to examine spatiotemporal changes in water bodies and vegetation in the Nile swamps of southern Sudan. Similarly, Soliman and Soussa (2011) applied multitemporal satellite imagery to detect wetland changes in the same region. In addition, Petersen and Fohrer (2010) explained the flooding and drying mechanisms of the seasonal Sudd floodplains along the Bahr El Jebel and showed that river spill is the principal driver of floodplain inundation, while evapotranspiration plays a major role in seasonal drying.

More recent research has advanced this field through the use of MODIS, Landsat, and other satellite products to classify land cover, map wetland inundation, and assess vegetation–water interactions over time. For example, Di Vittorio and Georgakakos (2018) developed a MODIS-based framework for land cover classification and wetland inundation mapping in the Sudd. Later, Di Vittorio and Georgakakos (2021) incorporated satellite-derived inundation and climatic data into hydrologic modeling of the wetland. Recent studies have also used long-term satellite observations to reconstruct wetland dynamics and detect changes in vegetation and surface water (Hardy et al., 2023; Persico et al., 2024). In addition, Lemenkova (2023) applied image segmentation techniques to classify the Sudd wetlands using GIS-based analysis. Together, these studies confirm that remote sensing provides an effective basis for monitoring landscape dynamics in the Sudd–Bahr El Jebel system.

Despite these advances, much of the published literature has focused primarily on the Sudd wetland core or on inundation dynamics, rather than on a broader basin-scale assessment of land cover changes across the Bahr El Jebel Basin as a whole (Di Vittorio & Georgakakos, 2018, 2021). In addition, many studies have emphasized hydrology, evaporation, or flood extent, while comparatively less attention has been given to the spatial and temporal transformation of major land cover classes across the wider basin (NBI, 2020). This reveals a clear research gap, particularly for studies seeking to connect basin-scale land cover dynamics with the environmental behavior of the Sudd and its surrounding floodplain landscape (Hardy et al., 2023).

Therefore, this study investigates spatiotemporal land cover changes in the Bahr El Jebel Basin using remote sensing. It aims to identify the major land cover classes, examine how these classes have changed over time, and provide a basin-scale perspective on landscape dynamics in an environmentally sensitive part of the Upper Nile. By building on previous studies conducted in the Sudd area while extending the analysis to the broader Bahr El Jebel Basin, this work seeks to contribute to a better understanding of wetland-related landscape

change and to support future hydrological and environmental assessments in the region (Persico et al., 2024; Hardy et al., 2023).

Study Area:

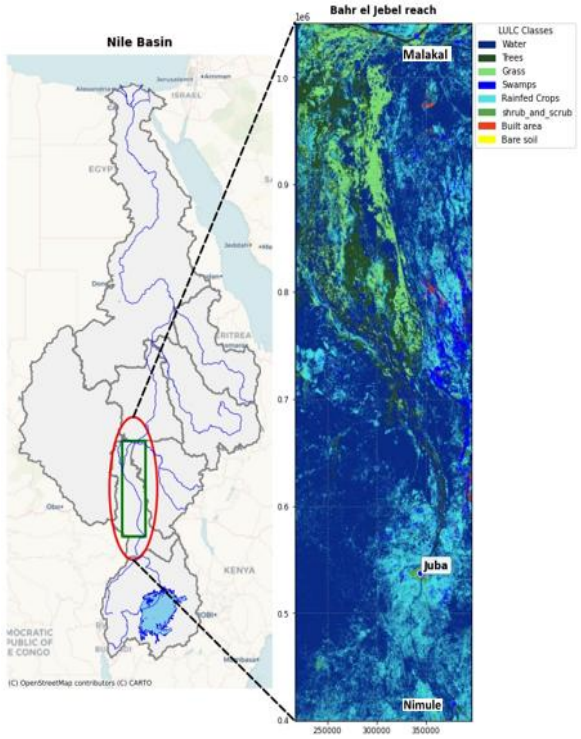

Fig. 1. Location of the Bahr El Jebel reach within the Nile Basin and the corresponding land use/land cover (LULC) classes (Dynamic World data set)

The Nile leaves the northern end of Lake Albert as the Albert Nile and flows for approximately 225 km toward Nimule through a wide, slow-moving, low-gradient reach bordered by swamps and lagoons; after crossing into South Sudan at Nimule, it is commonly known as Bahr El Jebel, or more broadly as part of the Upper White Nile (Salman, 2014; Sutcliffe & Parks, 1999). As shown in Fig. 1, the Bahr El Jebel reach considered in this study extends northward from Nimule through Juba to Malakal within the broader Nile Basin, and is characterized by a heterogeneous land-cover pattern dominated by water bodies, wetlands, swamps, grasslands, and shrublands. Downstream, this river system feeds the Sudd, one of the largest wetland complexes in the Nile Basin, with swamp and open-water extent often estimated at around 40,000 km², although the exact mapped area may vary depending on the delineation approach used (Mohamed et al., 2005; Nkwasa et al., 2024).

II. METHODOLOGY

The analysis is conducted at two complementary spatial scales: (i) the Bahr El Jebel Reach, where LULC changes are quantified; and (ii) the broader Equatorial Lakes sub-basin, whose rainfall patterns and lake storage dynamics are hypothesized to influence these changes.

The analytical workflow comprises eight sequential processing steps, beginning with data acquisition and continuing through LULC classification, change detection, climatological baseline development, anomaly assessment, and lake-level characterization. Table 2 summarizes each step, the platform used, and the main outputs generated.

Table 2. Analytical workflow overview.

Step / Description	Platform / Tool	Output
Dynamic World LULC acquisition — export yearly 10 m composites and per-class area statistics for 2015–2025	Google Earth Engine	GeoTIFF + CSV
CHIRPS rainfall download and clipping — acquire 420 monthly global GeoTIFFs and clip to each sub-basin shapefile	Python / rasterio	Clipped GeoTIFFs
WaPOR AETI retrieval — download dekadal actual evapotranspiration rasters at L2/L3 resolution	Python / wapordl	AETI GeoTIFFs
LULC change detection — detect flooded vegetation gain, loss, and persistence between year pairs	Python / rasterio	Change map + stats

Step / Description	Platform / Tool	Output
LULC–Rainfall–AETI correlation analysis — synthesise LULC area, rainfall, and AETI into a unified time series	Python / pandas	CSV + charts
Rainfall climatology computation — 30-year (1991–2020) monthly means per sub-basin (WMO standard)	Python / rasterio	12 monthly TIFFs
Rainfall anomaly calculation — absolute and percentage deviations from climatology; diagnostic maps	Python / matplotlib	Anomaly TIFFs + charts
Lake-level analysis — parse altimetry files, apply rolling means, and export publication figures	Python / pandas	PNG + Excel workbook

Annual Land Use and Land Cover composites for the Bahr El Jabel Reach were generated using the Google Dynamic World V1 product, which provides near-real-time 10 m Sentinel-2-based classifications into nine land cover classes (Brown et al., 2022). Processing was performed within the Google Earth Engine (GEE) cloud computing environment, with the Region of Interest (ROI) defined from an uploaded GEE asset representing the Bahr El Jabel Reach boundary shapefile. For each calendar year spanning 2015 to 2025, the Dynamic World Image Collection was filtered to the annual date range and spatially constrained to the ROI bounds. A mode composite of the 'label' band — representing the most frequently occurring land cover class per pixel — was then generated and clipped to the ROI. Mode compositing was adopted to reduce the influence of cloud contamination and phenological variability on the annual classification. Per-class pixel areas were subsequently computed using the ee.Image.pixelArea() function and normalized to feddans (1 feddan = 4,200 m²). Each annual composite was exported as a GeoTIFF at 10 m resolution in EPSG:32636, and area statistics were archived as comma-separated value (CSV) files. The nine Dynamic World classes are: Water (0), Trees (1), Grass (2), Flooded Vegetation (3), Crops (4), Shrub and Scrub (5), Built (6), Bare (7), and Snow and Ice (8). Flooded Vegetation (class 3) is designated as the primary indicator of hydrological forcing throughout this analysis.

The complete CHIRPS v3.0 monthly precipitation dataset spanning January 1991 to December 2025 — a total of 420 monthly fields — was acquired from the University of California Santa Barbara (UCSB) Climate Hazards Group data portal (Funk et al., 2015). Each GeoTIFF was downloaded via HTTP streaming with integrity verification, and a local cache of raw global grids was maintained to avoid redundant transfers across sub-basin processing iterations.

Following download, each monthly raster was spatially clipped to each of the four sub-basin boundaries — Lake Victoria, Lake Kyoga, Lake Albert, and the Bahr El Jabel Reach — using the rasterio masking module with the crop=True parameter. Sub-basin shapefiles were re-projected to the raster native coordinate reference system prior to masking. Clipped outputs were written as float32 GeoTIFFs with LZW compression and a designated nodata value of −9999, organised into per-basin subdirectories. This design separates the download step from the clipping step, ensuring that the 420 raw global GeoTIFFs are downloaded once and reused for all basin extractions.

Actual EvapoTranspiration and Interception (AETI) data were retrieved from the FAO Water Productivity through Open access of Remotely sensed derived data (WaPOR) platform using the wapordl Python library, which provides authenticated access to the FAO WaPOR API (FAO, 2020). Both Level 2 monthly AETI at approximately 250 m resolution (variable code L2-AETI-M) and Level 3 dekadal AETI at approximately 100 m resolution (variable code L3-AETI-D) were obtained as applicable. The region of interest was specified either as a bounding box or as a path to the study area GeoJSON boundary. The wapordl library

handled authentication, tiling, and mosaicking internally, and all retrieved rasters were archived in a designated output directory with unit conversions applied per the WaPOR convention (mm day^{-1}, mm dekad^{-1}, or mm month^{-1}). The AETI product serves as a proxy for vegetation water use, enabling detection of inundation-driven evapotranspiration signals within the LULC–hydrology interaction analysis.

Pixel-level changes in flooded vegetation (Dynamic World class 3) between successive annual composites were assessed using a binary change-detection approach in Python, employing the numpy and rasterio libraries. For each year pair, annual LULC GeoTIFFs were converted into flooded-vegetation masks, with Year 2 reprojected to the grid of Year 1 where required using nearest-neighbour resampling to preserve categorical values.

Annual LULC statistics, clipped CHIRPS rainfall grids, and WaPOR AETI data were integrated into a unified annual time-series dataset to examine the relationship between upstream hydro-climatological conditions and downstream LULC dynamics. Dynamic World area statistics were converted to a wide-format table by year and LULC class, while annual basin-average rainfall was calculated from clipped CHIRPS rasters using masked array averaging to exclude nodata pixels. Annual AETI totals were derived by aggregating dekadal raster means to yearly values. The three datasets were then merged by year into a single analysis dataframe. Flooded vegetation dynamics were compared with upstream rainfall and AETI using multi-variable time-series plots. Pearson correlation coefficients and 0–2-year lag analysis were applied to assess the strength and timing of the hydrological response between upstream climatic forcing and observed LULC changes in the Bahr El Jebel Reach.

The 30-year mean monthly rainfall climatology was computed for each sub-basin using the WMO standard reference period 1991–2020 as the baseline for anomaly assessment. Clipped CHIRPS rasters were screened by year and month from their filenames, retaining only files within this period. For each calendar month, the corresponding 30 annual rasters were stacked, and pixel-wise temporal means were calculated using masked array operations to exclude nodata values.

The resulting 12 monthly climatology rasters for each basin were exported as float32 GeoTIFFs, preserving the original coordinate reference system and spatial resolution, and named by basin and month abbreviation, such as {basin}_Jan.tif.

Monthly rainfall anomalies for the analysis period 2017–2025 were calculated relative to the 1991–2020 climatological baseline to identify periods of excess and deficit precipitation over the Equatorial Lakes sub-basins. For each basin, index dictionaries mapping (year, month) keys to observed CHIRPS raster paths, and month keys to climatology raster paths, were constructed programmatically. For each year–month combination within the analysis window, the corresponding climatology raster was reprojected to the observed raster grid using bilinear resampling, and anomalies were calculated pixel-wise as:

$$\text{Anomaly (mm)} = \text{Observed} - \text{Climatology}$$

$$\text{Anomaly (\%)} = (\text{Anomaly} / \text{Climatology}) \times 100$$

Anomaly rasters were partitioned into positive and negative sub-folders. For each month, a four-panel diagnostic map was generated comprising: (a) observed rainfall, (b) climatological mean, (c) absolute anomaly rendered with a Red–Blue diverging colour palette, and (d) percentage anomaly. Basin spatial means were aggregated into monthly CSV time series, from which three summary charts were produced: a bar chart of monthly anomaly in millimetres, a bar chart of percentage anomaly, and a cumulative anomaly curve.

Satellite radar altimetry records for Lakes Albert, Kyoga, and Victoria were obtained from the USDA FAS/LEGOS Virtual Station database, covering multi-mission observations from TOPEX to Sentinel-3A and referenced to the EGM2008 geoid. The fixed-format text files were processed in Python using pandas, extracting mission, cycle, date, orthometric water level, and measurement error, while excluding invalid dates and fill values. The records were organized chronologically for each lake, resampled monthly, and smoothed using a 12-month centred rolling mean to highlight inter-annual trends. The results were presented in a three-panel figure showing observed levels, error ranges, rolling means, and mission labels, alongside an Excel workbook

containing formatted lake-specific sheets and a summary statistics sheet.

The linkage between external climatological forcing and downstream LULC change is evaluated through a converging line of evidence approach that integrates four complementary analytical threads Table 3. Convergence across these independent lines of evidence is taken as corroboration of the central hypothesis.

Evidence Thread	Analytical Method
LULC trend analysis	Annual flooded vegetation area (feddans) derived from Dynamic World plotted against time to identify expansion and contraction episodes.
Rainfall anomaly timeline	Monthly and seasonal anomalies for each Equatorial Lakes sub-basin compared against LULC change years to establish temporal correspondence.
Lake-level response	12-month rolling mean of lake altimetry compared with rainfall anomaly periods to confirm the hydrological transfer function between rainfall and lake storage.
AETI signal	Elevated AETI over flooded areas during anomalously wet years confirms that inundation extent — rather than land management — drives the observed LULC signal.
Lead–lag correlation	Pearson r computed between basin rainfall anomalies and downstream flooded vegetation area at lags of 0–2 years to estimate hydrological travel time.

All processing and analytical procedures were performed using Python 3.10 or later, with the exception of the LULC classification, which was conducted in the Google Earth Engine cloud-computing environment.

The methodological framework adopted in this study is organized into five interconnected analytical components, as illustrated in Fig. 2. These components include LULC dynamics mapping, annual rainfall climatology and anomaly assessment, upstream lake-level analysis, LULC change detection, and hydro-climatological linkage and lag analysis. Together, they provide an integrated workflow for examining land cover dynamics in the Bahr El Jebel Reach and linking them with upstream hydro-climatological conditions. The framework progresses systematically from data acquisition and preprocessing to classification, statistical analysis, spatial change detection, and interpretation of potential driving factors.

The workflow integrates multiple remote sensing and hydro-climatological datasets within a unified analytical structure. As shown in Fig. 2, Dynamic World data were processed in Google Earth Engine to generate annual LULC composites and quantify flooded vegetation dynamics, while CHIRPS rainfall, WaPOR AETI, and satellite altimetry lake-level records were processed in Python to characterize rainfall variability, evapotranspiration, and upstream lake storage changes. The final integration stage applies correlation and lag analysis to assess the potential influence of upstream rainfall and lake-level variability on downstream LULC changes within the Bahr El Jebel Reach.

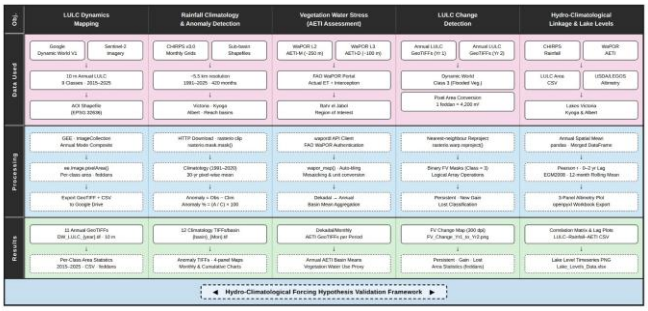

Fig. 2. Overall methodological framework of the study.

III. RESULTS

The Bahr El Jebel Basin experienced substantial year-to-year changes in flooded vegetation patterns, as indicated by the Dynamic World classification outputs between 2019 and 2025, as shown in Fig. 3. The observed changes were not linear, but rather reflected a sequence of rapid

expansion, partial stabilization, spatial redistribution, and localized contraction across the floodplain system. The most pronounced transformation occurred during 2019–2021, when newly detected flooded vegetation accounted for 61.5% of the total flooded-vegetation extent mapped in 2020 relative to 2019, and increased further to 69.5% of the total flooded-vegetation extent mapped in 2021 relative to 2020, while persistent areas remained relatively limited.

This suggests that the basin underwent an abrupt and widespread shift in the spatial extent of flooded vegetation rather than a gradual transition. During 2021–2023, the pattern began to change, as the proportion of persistent flooded vegetation increased to 44.8% and 48.9%, respectively, indicating that part of the earlier expansion had become more established. However, this was accompanied by increasing losses and continued emergence of new patches, which points to an active process of spatial reorganization rather than complete stability. In 2023–2025, the system continued to display marked variability, with losses peaking at 33.4% in 2023–2024 before persistence increased again to 49.5% in 2024–2025. These results highlight that flooded vegetation in the Bahr El Jebel Basin is highly dynamic and undergoes significant interannual fluctuations in both extent and spatial distribution. Accordingly, the present study investigates the main driver behind these observed land use/land cover changes in order to better understand the dominant processes shaping floodplain dynamics in the basin.

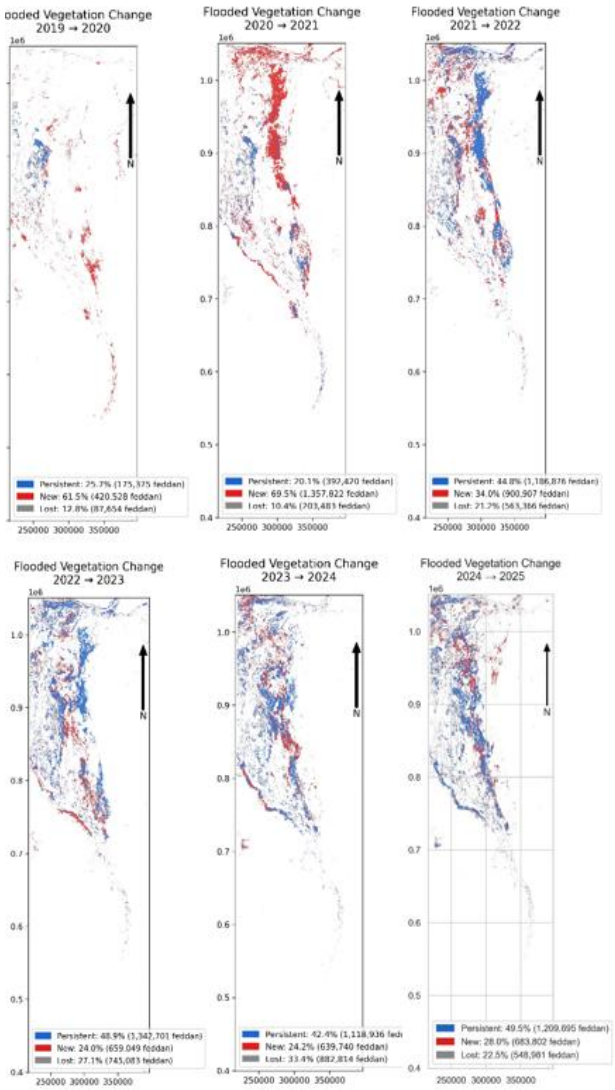

Fig. 3. Spatiotemporal changes in flooded vegetation across the Bahr El Jebel Basin during 2019–2025, showing persistent, newly gained, and lost flooded vegetation areas between consecutive years

Fig. 4 shows the annual trend of flooded vegetation area in the Bahr El Jebel Reach from 2015 to 2025. During the period 2015–2018, the flooded vegetation area remained relatively low and stable, ranging approximately between 0.25 and 0.35 million feddans. A moderate increase appeared in 2019, reaching about 0.55 million feddans, followed by a sharp expansion in 2020 to nearly 1.75 million feddans. The area continued to increase during 2021–2023, exceeding 2.0 million feddans, before showing a slight decline in 2024 and partial recovery in 2025.

Based on this trend, the period 2019–2020 was selected for detailed change-detection analysis because it represents the first major and most abrupt

expansion phase in flooded vegetation during the study period. This interval marks the transition from relatively limited flooded vegetation coverage before 2019 to a substantially larger wetland extent in 2020. Therefore, analyzing the spatial changes between 2019 and 2020 helps identify where the new flooded vegetation areas emerged and provides insight into the initial hydrological response that triggered the subsequent expansion across the floodplain system.

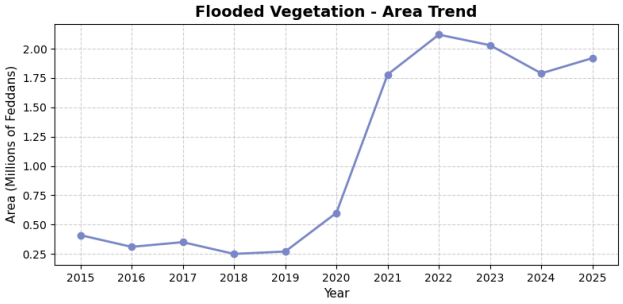

Fig.4. Annual trend of flooded vegetation area in the Bahr El Jebel Reach from 2015 to 2025

The rainfall anomaly maps for 2019 reveal clear seasonal and spatial variability across the Bahr El Jebel Reach relative to the 1991–2020 climatological baseline, as shown in Fig. 5. The blue tones indicate wetter-than-normal conditions, while the red tones represent rainfall deficits. February shows relatively weak and spatially uneven anomalies, suggesting limited deviation from the long-term mean during the dry-season period. In contrast, June records the most pronounced positive rainfall anomaly across most of the study area, indicating a wetter-than-normal onset of the main rainy season. Positive anomalies remain evident in September and November, although some localized negative patches appear, reflecting spatial differences in rainfall distribution across the reach.

These rainfall conditions provide an important hydro-climatological context for interpreting the observed LULC changes, particularly the expansion of swamp and flooded vegetation classes. Increased rainfall can enhance runoff generation, soil moisture, and floodplain inundation, thereby supporting the persistence and spread of wetland-related land-cover classes. This interpretation is consistent with the hydrological behaviour of the Bahr El Jebel–Sudd system, where wetland dynamics are influenced by rainfall, evapotranspiration, and upstream inflows from the Equatorial Lakes system (Mohamed & Savenije, 2014; Rebelo et al., 2012). Similar findings have also been reported in previous Sudd studies, where wetland expansion and land-cover change were linked to hydro-climatic variability and flood-pulse dynamics (Di Vittorio & Georgakakos, 2018; Hardy et al., 2023; Persico et al., 2024).

Based on these results, 2019 can be interpreted as a key transition year within the 25-year study period. The widespread positive rainfall anomalies observed during the main rainy season coincide with the beginning of a marked shift in wetland-related LULC patterns, especially the expansion of swamp and flooded vegetation classes. Accordingly, 2019 is highlighted as a reference year to explain the onset of these major changes and to examine their subsequent hydrological and land-cover responses across the Bahr El Jebel Reach.

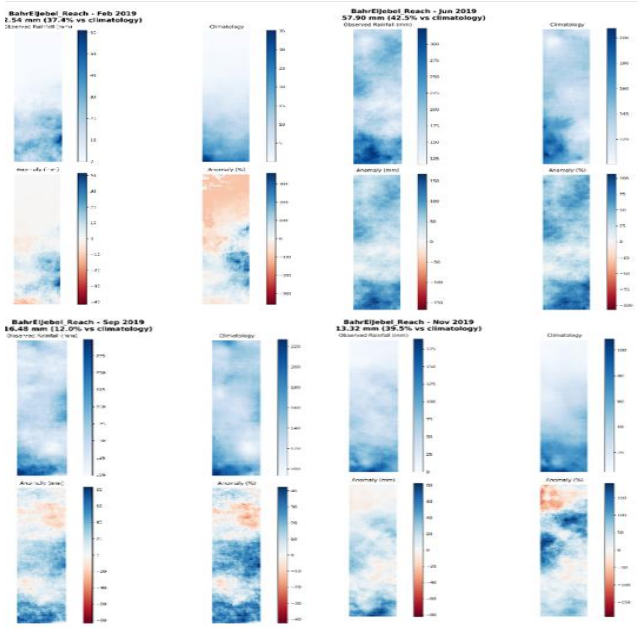

Fig. 5. Monthly rainfall anomalies over the Bahr El Jebel reach in 2019 relative to the 1991–2020 climatology.

Clear seasonal contrast between precipitation and evapotranspiration in the flooded vegetation zone of the Bahr El Jebel reach during 2015–2025 as shown in Fig.6. as rainfall is highly seasonal, with short wet-season peaks, whereas evapotranspiration remains relatively high for most of the year. Consequently, water surplus (P > ET) is limited to the rainy season, while water deficit (ET > P) prevails during most dry months. This suggests that local rainfall contributes to seasonal wetland expansion, but is not sufficient

by itself to maintain flooded vegetation throughout the year. The persistence of swamp and flooded vegetation therefore appears to depend not only on rainfall, but also on upstream inflows.

The precipitation–evapotranspiration balance over the flooded vegetation zone in the Bahr El Jebel reach indicates that evapotranspiration exceeds precipitation during most months of the year, while water surplus conditions are limited to short wet-season peaks. This suggests that local rainfall alone is not sufficient to sustain flooded vegetation throughout the year, and that the persistence and expansion of swamps and flooded vegetation depend on the combined influence of seasonal rainfall, upstream inflows, and floodplain water storage. This interpretation is consistent with previous studies in the Sudd region, which showed that direct rainfall represents only a limited component of the wetland water balance, while evapotranspiration constitutes a major hydrological loss term (Mohamed & Savenije, 2014). It also agrees with the findings of (Petersen and Fohrer 2010), who reported that flooding in the seasonal Sudd floodplains is driven mainly by river spill, and drying is controlled largely by evapotranspiration. Similarly, (Rebelo et al. 2012) emphasized the importance of the annual flood pulse in sustaining the hydrological functioning of the Sudd, while more recent satellite-based studies confirmed that wetland extent and land-cover dynamics in the Sudd–Bahr El Jebel system are strongly influenced by the interaction among rainfall, evapotranspiration, and upstream hydrological inputs (Di Vittorio & Georgakakos, 2018, 2021).

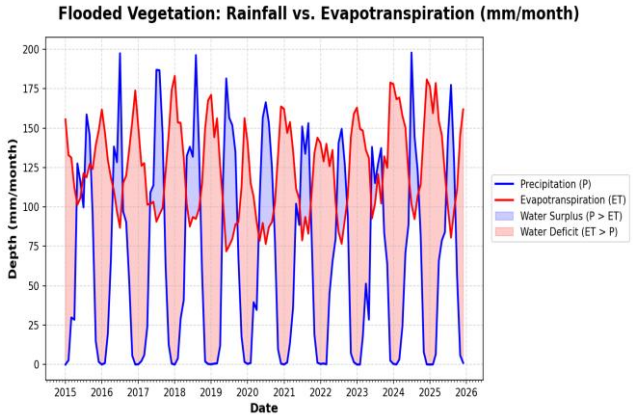

Fig. 6. Monthly precipitation–evapotranspiration balance over the flooded vegetation zone in the Bahr El Jebel reach during 2015–2025

The rainfall anomaly maps for the Equatorial Lakes sub-basin is indicate generally wetter-than-normal conditions, with clear temporal and spatial variability as shown in Fig .7. In May, the anomaly pattern was mixed, with positive anomalies concentrated mainly in the central basin. In June, positive anomalies became more widespread, and this wet signal strengthened further in October and December, when most of the basin showed above-normal rainfall. Overall, the results suggest that 2019 was a distinctly wet year across much of the Equatorial Lakes sub-basin.

These positive rainfall anomalies help explain the pronounced LULC changes observed in the basin and downstream areas. Higher rainfall likely increased runoff, lake inflow, and basin water storage, which supported the expansion of water-related and wetland-related land-cover classes. The persistence of positive anomalies from mid- to late 2019 suggests a sustained hydrological recharge phase rather than isolated wet events, making 2019 a key year in driving the observed landscape changes.

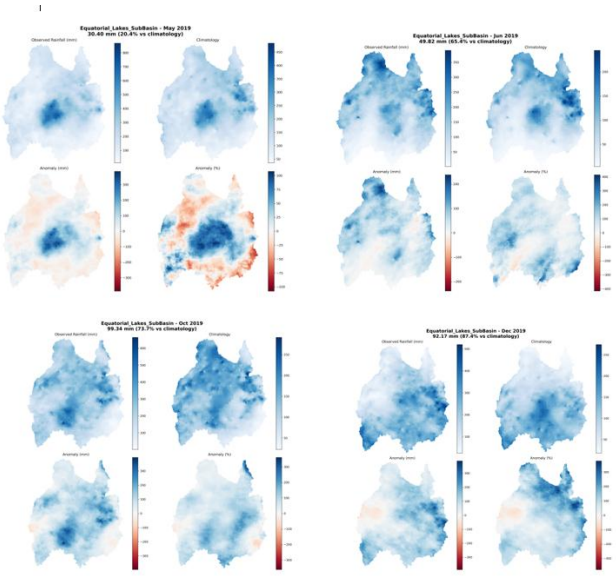

Fig. 7. Monthly rainfall anomaly maps for selected months in 2019 over the Equatorial Lakes sub-basin relative to the 1991–2020 climatology.

The cumulative rainfall anomaly in the Equatorial Lakes sub-basin reveals a marked transition toward persistently wetter-than-normal conditions starting

in late 2019. Between 2017 and 2019, the cumulative anomaly remained close to zero, reflecting alternating wet and dry periods and generally near-average rainfall conditions. In contrast, from the end of 2019 onward, a strong and nearly continuous upward increase, indicating the persistence of positive rainfall anomalies over several consecutive years as shown in Fig .8.

This wet phase continued through 2020–2025, with cumulative anomalies surpassing 1000 mm and remaining at elevated levels thereafter. Such a pattern suggests that the basin underwent a prolonged period of hydrological recharge rather than a short-lived rainfall event. As a result, the sustained rainfall surplus likely increased lake storage and enhanced downstream inflows, which in turn helps explain the significant expansion of water-related and wetland-related land-cover classes observed after 2019.

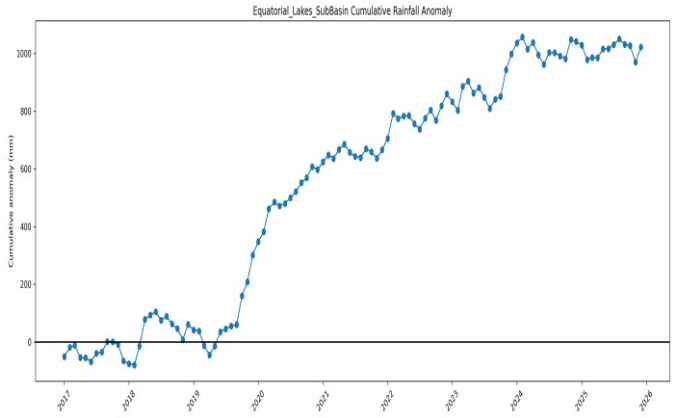

Fig .8. Cumulative rainfall anomaly in the Equatorial Lakes sub-basin during 2017–2025

The temporal evolution of satellite altimetry-derived water levels in Lakes Albert, Kyoga, and Victoria indicates a clear rise in lake storage during the recent wet phase, particularly since 2019, as shown in Fig. 6. To better identify the underlying hydrological trend, a 12-month rolling mean was applied in order to smooth short-term variability and reduce the influence of seasonal fluctuations and temporary oscillations. The smoothed curves show that Lake Albert experienced a marked increase beginning around 2020, with elevated levels during 2021 and again in 2024–2025. Lake Kyoga also displays a clear upward shift after 2020, followed by persistently high levels in the subsequent years. Similarly, Lake Victoria records a noticeable increase from around 2020 and maintains relatively high levels thereafter. Overall, the rolling mean confirms that these increases do not represent isolated seasonal peaks, but rather a sustained hydrological recharge phase in the Equatorial Lakes system. This rise in lake levels is hydrologically important because it suggests stronger downstream support to the Bahr El Jebel and Sudd system, helping to explain the observed expansion of wetland and flooded vegetation classes.

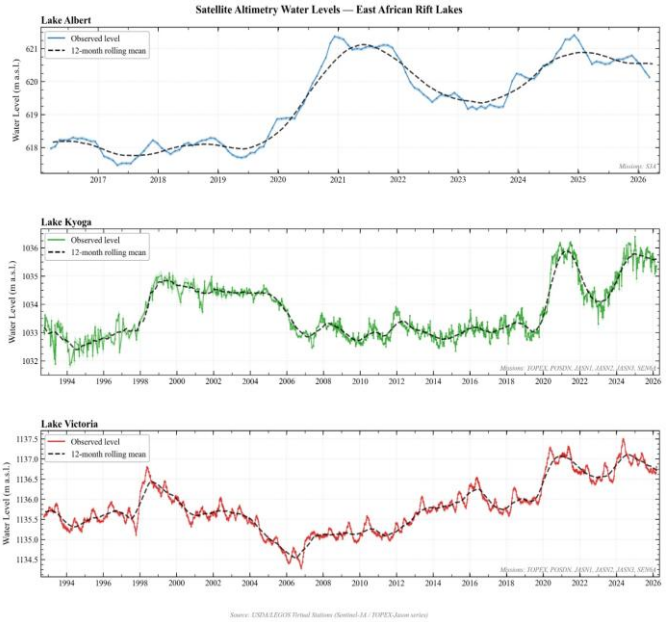

Fig. 9. Temporal evolution of satellite altimetry-derived water levels in Lakes Victoria, Kyoga, and Albert, including 12-month rolling mean curves.

The rise in satellite altimetry water levels shown in Fig. 9. is consistent with previous research on the Equatorial Lakes system, which indicates that the lakes entered a sustained high-water phase beginning around 2019–2020. In particular, Lake Victoria experienced an exceptional rise during 2019–2020, with satellite-based studies reporting an increase of about 1.4 m, mainly associated with unusually wet conditions and increased basin storage (Khaki et al., 2021). This broader regional signal is also reflected in Lake Kyoga and Lake Albert, where recent analyses describe prolonged high stages, delayed recession, and continued storage effects across the Victoria–Kyoga–Albert cascade, rather than isolated short-term peaks (Mulangwa et al., 2025). Consistent with this interpretation, regional

monitoring reports recorded very high lake levels during the recent flood period, including the highest recorded levels for Lake Kyoga in December 2020, Lake Albert in December 2020, and Lake Victoria in May 2021.

IV. CONCLUSION

This research demonstrates that the Bahr El Jebel Basin experienced significant spatiotemporal land cover changes, with the most pronounced transformations observed in swamp and flooded vegetation classes. The results identify 2019 as a critical turning point, marking the onset of a substantial shift in wetland-related land cover dynamics across the study area.

The hydro-climatic analysis indicates that this shift was closely associated with a sustained wet phase that developed after 2019 in both the Bahr El Jebel reach and the Equatorial Lakes sub-basin. Positive rainfall anomalies over the Equatorial Lakes were accompanied by rising lake levels in Lakes Victoria, Kyoga, and Albert, reflecting enhanced upstream storage and stronger downstream hydrological support. These conditions likely increased the volume of water transferred toward the Bahr El Jebel–Sudd system and created favorable conditions for wetland expansion.

The results further show that local rainfall alone cannot fully explain the persistence and expansion of flooded vegetation in the Bahr El Jebel Basin. Since evapotranspiration exceeded precipitation during most months of the year, the maintenance of flooded vegetation cannot be attributed solely to local water inputs. Instead, the findings suggest that the dominant control on flooded vegetation expansion was external, driven primarily by upstream inflows from the Equatorial Lakes system, with local rainfall acting as a secondary supporting factor. Therefore, the recent increase in flooded vegetation should be understood mainly as a response to basin-scale hydrological forcing rather than to local climatic conditions alone.

V. FUNDING

This research did not receive any specific grant from funding agencies in the public, commercial, or not-for profit sectors.

REFERENCES

[1] Birkett, C. M., Ricko, M., & Yang, H. (2025). Algorithm theoretical basis document (ATBD) for along-track inland surface water level products as derived from short-repeat satellite radar altimeters (Version 1.0, NASA/TM-20250005550). NASA Goddard Space Flight Center. https://ntrs.nasa.gov/citations/20250005550

[2] Birkett, C. M., Reynolds, C., Beckley, B., & Doorn, B. (2011). Real-time monitoring of regional lake and reservoir variations from satellite radar altimetry. International Journal of Remote Sensing, 32(19), 5405-5425. (Source: Global Water Monitor, NASA GSFC).

[3] Brown, C. F., Brumby, S. P., Guzder-Williams, B., Birch, T., Brooks Hyde, S., Mazzariello, J., Czerwinski, W., Pasquarella, V. J., Haertel, R., Ilyushchenko, S., Schwehr, K., Weisse, M., Stolle, F., Hanson, C., Guinan, O., Moore, R., & Tait, A. M. (2022). Dynamic World, near real-time global 10 m land use land cover mapping. Scientific Data, 9, 251. https://doi.org/10.1038/s41597-022-01307-4

[4] Climate Hazards Center. (2026). CHIRPS v3. University of California, Santa Barbara. https://www.chc.ucsb.edu/data/chirps3

[5] Denny, P. (1984). Permanent swamp vegetation of the Upper Nile. Hydrobiologia, 110, 79–90. https://doi.org/10.1007/BF00025778

[6] Di Vittorio, C. A., & Georgakakos, A. P. (2018). Land cover classification and wetland inundation mapping using MODIS. Remote Sensing of Environment, 204, 1–17. https://doi.org/10.1016/j.rse.2017.11.001

[7] Di Vittorio, C. A., & Georgakakos, A. P. (2021). Hydrologic modeling of the Sudd wetland using satellite-based data. Journal of Hydrology: Regional Studies, 37, 100922. https://doi.org/10.1016/j.ejrh.2021.100922

[8] FAO. (2021). The WaPOR database. Food and Agriculture Organization of the United Nations. https://www.fao.org/aquastat/en/geospatial-information/wapor/

[9] FAO. (n.d.). ETLook — pyWaPOR documentation. Food and Agriculture Organization of the United Nations. https://www.fao.org/aquastat/py-wapor/_etlook.html

[10] FAO (2023). WaPOR V3 Database: Quality Assessment and Technical Specifications. Food and Agriculture

Organization of the United Nations (FAO), Rome, Italy. https://data.apps.fao.org/wapor/

[11] Funk, C., Peterson, P., Landsfeld, M., Pedreros, D., Verdin, J., Shukla, S., Husak, G., Rowland, J., Harrison, L., Hoell, A., & Michaelsen, J. (2015). The climate hazards infrared precipitation with stations—A new environmental record for monitoring extremes. Scientific Data, 2, 150066. https://doi.org/10.1038/sdata.2015.66

[12] Google Earth Engine Data Catalog. (2026). Dynamic World V1.https://developers.google.com/earth-engine/datasets/catalog/GOOGLE_DYNAMICWORLD_V1

[13] Hardy, A., Palmer, P. I., & Oakes, G. (2023). Satellite data reveal how Sudd wetland dynamics are linked with globally significant methane emissions. Environmental Research Letters, 18(7), 074044. https://doi.org/10.1088/1748-9326/ace272

[14] Khaki, M., & Awange, J. (2021). The 2019–2020 rise in Lake Victoria monitored from space: Exploiting the state-of-the-art GRACE-FO and the newly released ERA-5 reanalysis products. Sensors, 21(13), 4304. https://doi.org/10.3390/s21134304

[15] Lemenkova, P. (2023). Image segmentation of the Sudd wetlands in South Sudan for environmental analytics by GRASS GIS scripts. Analytics, 2(3), 745–780. https://doi.org/10.3390/analytics2030040

[16] Mohamed, Y. A., & Savenije, H. H. G. (2014). Impact of climate variability on the hydrology of the Sudd wetland: Signals derived from long term (1900–2000) water balance computations. Wetlands Ecology and Management, 22(2), 191–198. https://doi.org/10.1007/s11273-014-9337-7

[17] Mohamed, Y. A., van den Hurk, B. J. J. M., Savenije, H. H. G., & Bastiaanssen, W. G. M. (2005). The impact of the Sudd wetland on the Nile hydroclimatology. Water Resources Research, 41(8), W08420. https://doi.org/10.1029/2004WR003792

[18] Mulangwa, D., Naturinda, E., Koboji, C., Zaake, B. T., Black, E., Cloke, H., & Stephens, E. M. (2025). Lake Victoria to the Sudd Wetland: Flood wave timing, connectivity and wetland buffering across the White Nile [Preprint]. EGUsphere. https://doi.org/10.5194/egusphere-2025-5009

[19] NASA Earth Observatory. (2021, June 10). Lake Victoria's rising waters. NASA. https://science.nasa.gov/earth/earth-observatory/lake-victorias-rising-waters-148414/

[20] NASA Global Water Measurements. (2026). Water measurements: Lakes and reservoirs. NASA Goddard Space Flight Center. https://earth.gsfc.nasa.gov/gwm/lake/Index

[21] Nile Basin Initiative. (2020). Sudd wetland monograph–Volume 1: Overview of the Sudd wetland–ecosystems and land use. Nile Basin Initiative. https://nilebasin.org/sites/default/files/2023-09/Sudd%20Wetland%20Monograph%20%E2%80%93%20Volume%201%20Overview%20of%20the%20Sudd%20Wetland%20and%20Land%20Use.pdf

[22] Nkwasa, A., Chawanda, C. J., Schlemm, A., Ekolu, J., Frieler, K., & Van Griensven, A. (2024). Historical climate impact attribution of changes in river flow and sediment loads at selected gauging stations in the Nile basin. Climatic Change, 177, 42. https://doi.org/10.1007/s10584-024-03702-9

[23] Persico, G., Seyoum, W. M., & Peterson, E. W. (2024). Interrelationships between NDVI, surface water, and regional hydro-climatic variables in the Sudd wetland. Wetlands, 44, 92. https://doi.org/10.1007/s13157-024-01851-2

[24] Petersen, G., Abeya, J. A., & Fohrer, N. (2007). Spatio-temporal water body and vegetation changes in the Nile swamps of southern Sudan. Advances in Geosciences, 11, 113–116. https://doi.org/10.5194/adgeo-11-113-2007

[25] Petersen, G., & Fohrer, N. (2010). Flooding and drying mechanisms of the seasonal Sudd flood plains along the Bahr El Jebel in southern Sudan. Hydrological Sciences Journal, 55(1), 4–16. https://doi.org/10.1080/02626660903525278

[26] Pietroiusti, R., Vanderkelen, I., Otto, F. E. L., Barnes, C., Temple, L., Akurut, M., Bally, P., van Lipzig, N. P. M., & Thiery, W. (2024). Possible role of anthropogenic climate change in the record-breaking 2020 Lake Victoria levels and floods. Earth System Dynamics, 15(2), 225–264. https://doi.org/10.5194/esd-15-225-2024

[27] Rebelo, L.-M., Senay, G. B., & McCartney, M. P. (2012). Flood pulsing in the Sudd wetland: Analysis of seasonal variations in inundation and evaporation in South Sudan. Earth Interactions, 16(1), 1–19. https://doi.org/10.1175/2011EI382.1

[28] Ricko, M., Birkett, C. M., & colleagues. (2024). The Global Water Monitor: Lake, wetland, and river reach monitoring for resource management and hazard observation. NASA Technical Reports Server. https://ntrs.nasa.gov/citations/20240010300

[29] Salman, S. M. A. (2014). Water resources in the Sudan North-South peace process and the ramifications of the secession of South Sudan. In E. Weinthal, J. Troell, & M. Nakayama (Eds.), Water and post-conflict peacebuilding (pp. 327–355). Earthscan. https://www.taylorfrancis.com/chapters/edit/10.4324/9781849775809-23/water-resources-sudan-north-south-peace-process-ramifications-secession-south-sudan-salman-salman

[30] Soliman, G., & Soussa, H. (2011). Wetland change detection in Nile swamps of southern Sudan using multitemporal satellite imagery. Journal of Applied Remote Sensing, 5(1), 053517. https://doi.org/10.1117/1.3571009

[31] Sutcliffe, J. V., & Parks, Y. P. (1999). The hydrology of the Nile. IAHS Press. https://www.hydrosciences.fr/sierem/Bibliotheque/biblio/hydrology%20of%20the%20Nile.pdf